A synthetic tripeptide as organogelator: elucidation of gelation mechanism †

Sudip Malik,[a] Samir K. Maji,[b] Arindam Banerjee *[b] and Arun K. Nandi *[a]

[a] *Polymer Science Unit, Indian Association for the Cultivation of Science, Jadavpur, Calcutta-700032, India. E-mail: psuakn@mahendra.iacs.res.in*
[b] *Department of Biological Chemistry, Indian Association for the Cultivation of Science, Jadavpur, Calcutta-700032, India. E-mail: bcab@mahendra.iacs.res.in; Fax: +91-33-473 2805; Tel: +91-33-473 4971*

Received (in Cambridge, UK) 19th December 2001, Accepted 2nd April 2002
First published as an Advance Article on the web 22nd April 2002

A new terminally protected synthetic tripeptide with noncoded amino acids, *tert*-butyloxycarbonyl-β-alanyl-α-aminoisobutyryl-β-alanyl methyl ester, is synthesized. The product is characterized by ^{1}H NMR and DQF COSY NMR data. This tripeptide produces thermoreversible gels in 1,2-dichlorobenzene (DCB) at room temperature (30 °C). The morphology of the dried gels is studied using optical microscopy, scanning electron microscopy (SEM) and transmission electron microscopy (TEM). The micrographs show the presence of both rod like morphology and liquid–liquid phase separated morphology in the gels. Thermal study by differential scanning calorimeter (DSC-7) indicates the presence of a reversible first order phase transition during heating and cooling processes. Wide-angle X-ray scattering (WAXS) and electron diffraction experiments indicate the presence of polycrystalline materials in the gel and the crystal structure of the gel is almost the same as that of the pure tripeptide. Solvent subtracted Fourier transformed infra-red (FT-IR) study indicates that in the sol state there are free N–H and intramolecular hydrogen bonded N–H stretching vibrations at 3440 and 3375 cm^{-1}, respectively. In the gel state both these vibrations shifted to 3325 and 3309 cm^{-1}, respectively. The phase diagram of these gels, determined from both the DSC method and visually, indicates the tripeptide–DCB complexation with singular point characteristics. An attempt is made to understand the gelation mechanism of this system by measuring the gelation rate (t_{gel}^{-1}) using the test tube tilting method. The gelation rate (t_{gel}^{-1}) is expressed as $t_{gel}^{-1} \propto f(C)f(T)$ and the analysis of the concentration function $f(C)$ at a particular temperature indicates that the gelation process obeys the three dimensional percolation mechanism. The microscopic mechanism of the gelation process is explored from the temperature function $f(T)$ of the gelation rate at a particular concentration expressing $f(T)$ in two different forms: (I) for fibrillar (rod like) crystallization and (II) for spinodal decomposition. A tentative structure of the tripeptide in the gel state has been proposed by molecular modeling using the MMX program.

Introduction

The formation of organogels is one of the finest examples of a supramolecular self-assembly process.[1,2] Ghadiri and his co-workers established that self-assembly of cyclic β-peptides (oligomers of β-amino acids) leads to the formation of nanotubular structures which function as artificial transmembrane ion channels.[3] Supramolecular self-assembly formation completely depends upon reversible non-covalent interactions.[2,4,5] A main problem for supramolecular assembly is the maintenance of a rapid equilibrium between the assembled and disassembled structure. In order to overcome the problem, many groups offer various solutions like crystal engineering,[6,7] preparation of soluble or solvent-stable aggregates[1,2,8–12] and hydrogen-bonding interactions.[1,2] Peptides containing β-amino acids are excellent candidates for foldamers[12] due to their surprising secondary structure forming propensities in organic solvents, in water and in the solid state. Seebach *et al.* and Gellman *et al.* showed that acyclic β-peptides (oligomers of homo/hetero β-amino acids) can adopt spectacular secondary and super-secondary structures like 12-helices,[13] 14-helices,[14] and new β-hairpins[15] which are unprecedented in the naturally occurring proteins. Cyclic β-peptides with β-substituted, chiral β-amino acids and cyclic peptides composed of alternating D- and L-α-amino acids can adopt flat ring conformations and they can stack in the solid state by backbone–backbone intermolecular hydrogen bonding to form hollow tubular ensembles.[16] The main forces responsible for supramolecular self-assembly are (1) hydrogen-bonding,[1,2] (2) polar and van der Waals interactions,[1,2] (3) π–π stacking[17] and (4) crystallization.[7,18] The control of gelation phenomena and the design of novel types of organogelators are challenging, particularly in the field of short peptides.

From the above-mentioned approach we may design a new type of organogelator (peptide containing noncoded amino acids) which can satisfy the criteria of self-aggregation and gelation. The geometry of the building blocks and their arrangements in space, and the nature of the hydrogen-bonding are mainly responsible for the structure and properties of macromolecular self assembled ensembles. Rigid peptides using conformationally constrained amino acid residues give rise to a particular arrangement which remains unaltered in solution with change in temperature, solvent and composition, but a molecule with only flexible residues would not yield a definite structure in solution. However, if one designs a peptide having both conformationally rigid and conformationally flexible residues it may produce varieties of structures depending on solvent, composition, temperature, *etc*.[19] So in this last category

† Electronic supplementary information (ESI) available: the 500 MHz 1-D ^{1}H NMR spectrum, the 500 MHz ^{1}H–^{1}H DQF COSY spectrum of the tripeptide in $CDCl_3$ and the MALDI-MS spectrum of the tripeptide. See http://www.rsc.org/suppdata/p2/b1/b111598g/

Table 1 ^{1}H NMR parameters for the tripeptide in $CDCl_3$ (the ^{1}H–^{1}H DQF COSY spectrum for the tripeptide is submitted as supplementary material)

Residue	NH δ (ppm)	$C^{\alpha}H$ δ (ppm)	$C^{\beta}H$ δ (ppm)
β-Ala(1)	5.59	3.38–3.40	2.40–2.42
Aib(2)	6.27	—	1.51
β-Ala(2)	6.94	3.49–3.52	2.57–2.59

of samples it may be possible to design structures of different types and our interest is in constructing such a structure which can self assemble to produce gel. Here we design a peptide with two conformationally contrasting nonprotein (*i.e.*, noncoded) amino acids namely α-aminoisobutyric acid (Aib) and a β-amino acid, β-alanine (β-Ala). The former has a conformationally restricted nature and the latter has sufficient flexibility. This combination may form well-defined structures like foldamers. This type of acyclic peptide is a potent candidate to create a network structure through intermolecular aggregation in organic solvents due to the presence of hydrogen bond forming amide linkages. The intermolecular aggregation may also depend on the nature of the solvent. In this report we present such a study of aggregation/gelation for a terminally protected tripeptide, Boc-β-Ala-Aib-β-Ala-OMe in 1,2-dichlorobenzene (DCB). The N-terminal protection has been made with *tert*-butoxycarbonyl (Boc) and the C-terminal is made with methyl ester to solubilize the compound in organic solvents.

The mechanism of organogel formation is still poorly understood. The main objective of this study is, therefore, to establish a satisfactory gelation mechanism in this tripeptide gel. For this purpose we have undertaken morphological, structural, thermodynamic and kinetic approaches to elucidate the gelation mechanism. In the thermoreversible polymer gels it is now established that a three-dimensional percolation mechanism is satisfactorily obeyed and we want to investigate whether the percolation model is obeyed in this gel also. Besides, what is the structure of the peptide molecule in the gel—is it different from that in its solution state or in its solid state? How is the network structure formed? In this paper we want to present a comprehensive study of gelation in this system to address the above questions. Finally molecular modeling is also used to present a tentative structure of the tripeptide molecule in the gel. The tripeptide sample gels in 1,2-dichlorobenzene, monochlorobenzene and benzene, however it does not gel in chloroform, acetonitrile, isobutanol, *N*,*N*-dimethylformamide, diethyl succinate *etc*. Here we want to present a detailed mechanistic aspect of gelation taking 1,2-dichlorobenzene as a representative solvent.

Results and discussion

A. Characterization of the tripeptide

From ^{1}H NMR and 2D DQF-COSY experiments sequence specific assignments were done successfully. Important NMR parameters for the peptide are listed in Table 1. From the mass spectroscopic results it is shown that the observed mass at *m*/*z* 360 corresponds to a molecular ion peak (MH^+) which completely agrees with the calculated mass value (359). (Mass spectrum and NMR spectrum are supplied as supplementary material.)

B. Morphology of the gel

The tripeptide gels in 1,2-dichlorobenzene are turbid in all the compositions studied here. In Fig. 1(a–c) the morphology of the dried gel is shown from the optical microscopy, scanning electron microscopy and transmission electron microscopy, respectively. It is apparent from Fig. 1(a)–(c) that the network consists of rod like structures. However, from a careful look at these micrographs it appears that another type of network structure (marked by arrow) is superimposed on the rod like network structure. In Fig. 1(c) it is also apparent that some portions of the network structure are not exactly connected through rods. In Fig. 1(d) the polarized optical micrograph of the undried gel is shown. Here also two types of network morphology are clearly observed. So it may be argued that gel morphology studied in the dried state is the same as in the gel state. To elucidate the cause of the coexistence of two different types of network structures we have performed an X-ray diffraction study and a phase equilibrium study.

C. Structure

In Fig. 2 the WAXS pattern of dried gel (diffractogram a) is shown and here sharp crystalline peaks are clearly seen. To compare it with that of the pure tripeptide the WAXS pattern of pure tripeptide (diffractogram b) is also included in Fig. 2. From the two diffractograms it is clear that almost all the peaks (except a small peak at 12.9°) are the same for both the cases, indicating the crystal structure is the same both in the gel state and in the solid state. Thus it may be proposed that the rods seen in the micrographs consist of the tripeptide crystals and the crystallites are responsible for the formation of cross-linking junctions. To elucidate the nature of the cross-linking junctions we have also performed electron diffraction experiments, which gave the pattern shown in Fig. 3 where diffraction rings are present.[22] This indicates that crystallites producing the cross-linking junctions are polycrystalline in nature.[23]

D. Thermal study

To understand the nature of the other cross-linking pieces we performed a phase equilibrium study for a composition (1% w/v) where no gelation takes place, *i.e.*, below the critical gelation concentration. The solution was heated to 110 °C to make it homogeneous and kept at 25 °C for 12 h. A distinct phase separation into two layers was observed. Since there are some reports that liquid–liquid phase separation may also act as a cross-linking junction for polymers,[25,26] so it may be argued here that the liquid–liquid phase separation may also be responsible for the gelation process of this system. The different (non-rod) type of network structure observed in Fig. 1 (marked by arrow) may, therefore, occur due to liquid–liquid phase separation. Liquid–liquid phase separation may also be responsible for the cloudiness of the gel. So it appears from this result that it is a unique system where both liquid–liquid phase separation and crystallization of the tripeptide may be responsible for producing the gel. A detailed study of the phase diagrams will be presented in the following section.

In Fig. 4(a) thermograms of gels of differing tripeptide concentration for the heating process are shown. It is apparent from the figure that first order phase transition (*i.e.*, melting) peaks are observed in all the compositions. One of the important criteria of thermoreversible gelation is the existence of reversible first order phase transition.[8,27] In Fig. 4(b) the dynamic cooling thermograms of gels indicate the presence of exotherms in all the cases. So the presence of fibrillar network structure and reversible first order transition confirms that the tripeptide produces thermoreversible gel in 1,2-dichlorobenzene. However, the exotherms in Fig. 4(b) become broader with the increase in tripeptide concentration and this is probably due to the difficulty in the diffusion process of the tripeptide molecule with increasing concentration. For the solid tripeptide molecule the exothermic peak is absent because of a very slow crystallization rate due to the same reason. However, the pure sample crystallizes after keeping for a longer time at 50 °C. In Fig. 5 the gel melting temperatures (T_{gm}) and the gelation temperature (T_{gel}) are plotted with the weight fraction of the tripeptide ($W_{peptide}$) in the gels. The nature of the phase diagram is almost the same for both the processes; however,

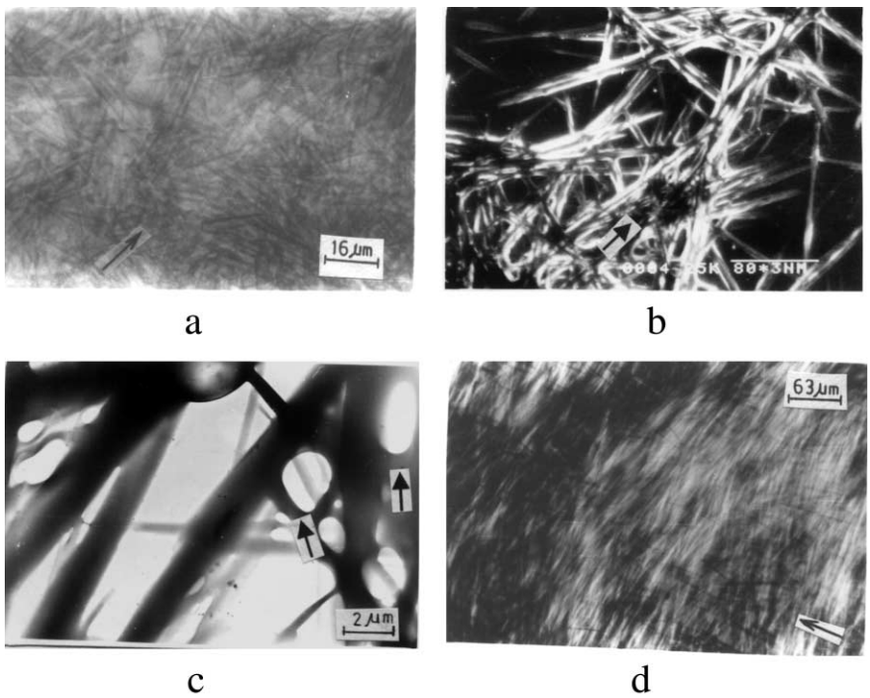

Fig. 1 Photomicrographs of dried gels of the tripeptide in 1,2-dichlorobenzene: (a) optical micrograph (5% w/v), (b) SEM (10% w/v), (c) TEM (1% w/v) and (d) polarized optical micrograph of undried gel (9% w/v). [Arrow in each micrograph indicates morphologies different from the rod like network structure].

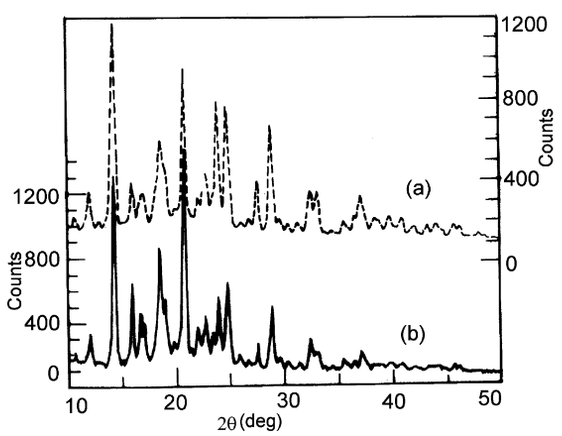

Fig. 2 WAXS pattern of (a) dried tripeptide gel (10% w/v) and (b) tripeptide crystal.

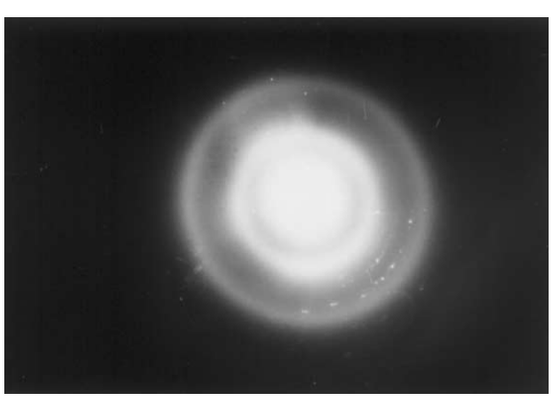

Fig. 3 Electron diffraction pattern of the dried tripeptide gel (1% w/v, camera length 0.8 m).

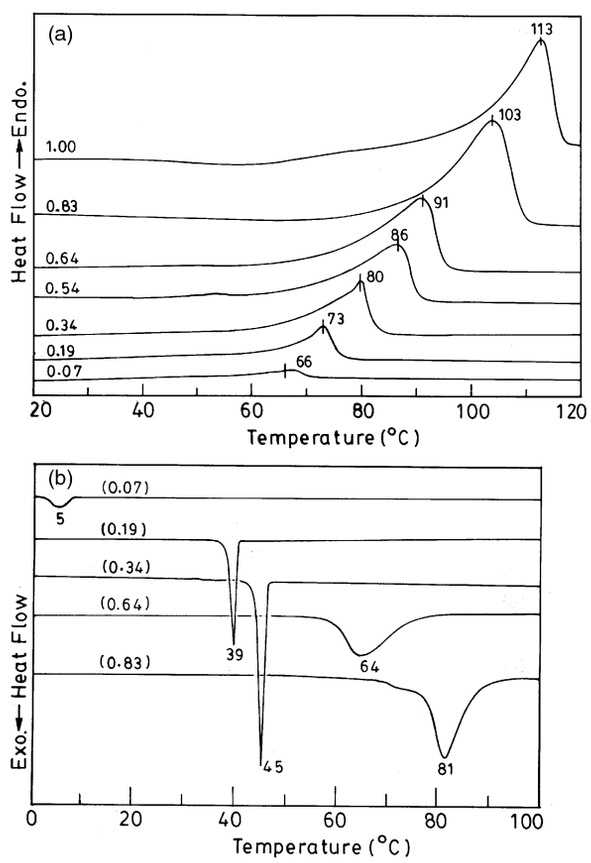

Fig. 4 (a) DSC thermograms of tripeptide–DCB gels prepared at 15 °C for the indicated weight fractions of the tripeptide ($W_{peptide}$) in the gel (heating rate 10 °C min^{-1}). (b) DSC thermograms for cooling of the tripeptide–DCB sols from 110 °C at the scan rate 5 °C min^{-1} for the indicated weight fractions of the tripeptide ($W_{peptide}$).

there is a hysteresis effect (60–20 °C) which varies for varying tripeptide concentration, the lower tripeptide content gel having a higher hysteresis effect. In order to observe the gel melting phenomena visually we have also performed the experiment in sealed glass tubes. In the experiment it has been observed that at peptide concentrations, $W_{peptide} \leq 0.27$ the gel breaks (*i.e.*, melts) before it becomes transparent. The sol becomes transparent at temperatures (T_s) which are a few degrees higher than the respective gel melting temperatures. The difference between

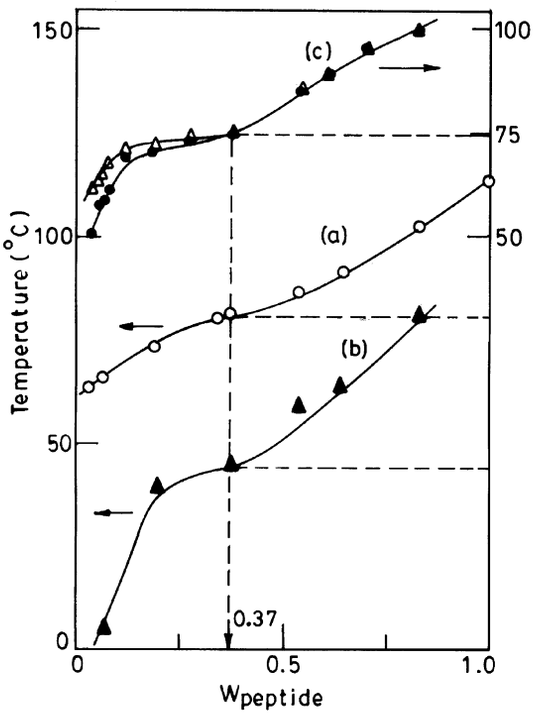

Fig. 5 Phase diagram of the tripeptide–DCB gel, obtained from (a) DSC, heating experiment (T_{gm}), (b) DSC, cooling experiment (T_{gel}) and (c) visual method, (●) gel melting temperature (T'_{gm}) and (△) turbidity disappearance temperature (T_s) (see text).

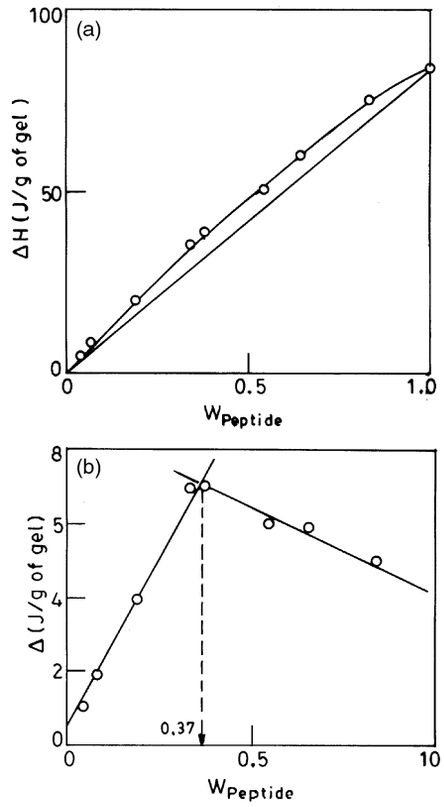

Fig. 6 (a) ΔH *vs.* $W_{peptide}$ plot for the gel melting process in DSC. (b) Deviation (Δ) *vs.* $W_{peptide}$ plot for the tripeptide–DCB gel.

T'_{gm} and T_s decreases with increase in $W_{peptide}$ and at $W_{peptide} \geq 0.40$ the T'_{gm} and T_s are almost the same. Thus it appears that if a sol is cooled, it first passes the liquid–liquid phase separation boundary and then it becomes gel, particularly for lower concentrations ($W_{peptide} \leq 0.27$).

Now we analyze the ΔH values obtained during heating. The ΔH *vs.* $W_{peptide}$ plot is shown in Fig. 6(a) and it shows a positive deviation from linearity joining the line between the two components. The enthalpy of gel melting may be considered to consist of three contributions:[7,18b]

$$\Delta H^{(per\ gm)} = w_1\Delta H_1 + w_2\Delta H_2 + \Delta H_c \quad (1)$$

Where w represents the weight fraction and subscripts 1 and 2 represent the solvent, DCB, and the tripeptide, respectively. ΔH_i represents the enthalpy of each component and ΔH_c is the enthalpy of melting of any tripeptide–solvent assembled (*i.e.*, complex) structure, if formed during gelation. Since DCB does not crystallize at the gelation temperature (15 °C) so ΔH_1 may be considered as zero. Consequently,

$$\Delta H - w_2\Delta H_2 = \Delta H_c \quad (2)$$

The left hand side of eqn. (2) is the positive deviation (Δ) from linearity (Fig. 6a). The deviation (Δ) is plotted with $W_{peptide}$ (Fig. 6b) and it shows a maximum which indicates that there is tripeptide–DCB complex formation in this gel.[7,8,18,28] The maximum ($W_{peptide}$ = 0.37) corresponds to the composition of the tripeptide–solvent complex formed during gelation. The molar ratio of DCB and tripeptide comes out as 4 : 1 at this composition. The nature of the complex is not known, but it may be postulated that it occurs through the physical interaction between four >C=O groups of the tripeptide and the benzene ring of DCB. The phase diagrams shown in Fig. 5 may be explained in analogy with the phase diagrams of poly(vinylidene fluoride)–solvent gels.[7,18] All the phase diagrams are characteristic in that they have a singular point.[28,29] The above phase diagrams are drawn from the endotherms or exotherms which show a single peak. No separate peak for the compound formation occurs in thermograms for any of the compositions. So it may be considered that the exotherms or endotherms are composed of two indistinguishable peaks, the first of which corresponds to the transformation of

$$\text{compound} \longrightarrow \text{solid} + \text{solvent} \quad (3)$$

and is nonvariant with composition. This is shown by a dotted line (Fig. 5). The second peak is due to the melting of the

$$\text{solid} \longrightarrow \text{liquid} \quad (4)$$

and it varies with composition as shown in the diagrams.[18] Thus the thermal study indicates that there are both liquid–liquid phase separation and tripeptide–solvent complex formation in this system.

E. FT-IR study

In Fig. 7 the FT-IR spectra of solvent subtracted gel (a) and also the pure solid tripeptide (b) are shown. It is apparent from the figure that both the spectra are almost identical and this indicates that the gel structure and the solid crystal structure are the same. This is in accordance with the WAXS results discussed earlier. So it proves that during drying of the gel tripeptide crystal structure (*i.e.* polymorphic nature) doesn't change. The solvent subtracted spectrum of a 0.3% (w/v) solution of tripeptide in 1,2-dichlorobenzene (c) is shown. This spectrum is completely different from that of the pure tripeptide or its gel. In this spectrum (c) there are N–H stretching peaks at 3440 and 3375 cm^{-1}. The former peak is due to the free N–H vibration whereas the 3375 cm^{-1} peak is for the hydrogen bonded (intramolecular) N–H stretching vibration.[30,31] However, in FT-IR spectra (a) and (b) these peaks are completely

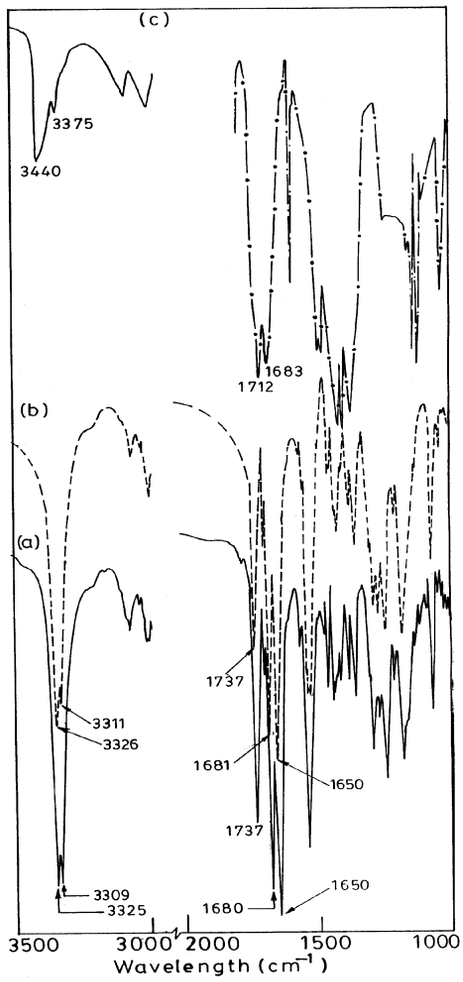

Fig. 7 FT-IR spectra of (a) solvent subtracted tripeptide gel in DCB (10% w/v), (b) pure tripeptide sample and (c) tripeptide solution in DCB (0.3% w/v).

absent and new peaks at 3325 and 3309 cm^{-1} appear. So in gel or in the solid crystalline state the molecular arrangement makes all the N–H bonds bound and it probably occurs through the intermolecular hydrogen bonding. This intermolecular association through H-bonding makes the system crystallize in the form of rods.

From the FT-IR spectrum (c) it is apparent that there are two peaks (1712 and 1683 cm^{-1}) for the >C=O stretching characterizing the ester and amide carbonyl groups, respectively.[30,31] However, in the gel or in the pure solid form these peaks are not observed, rather the peaks at 1737, 1680 and 1650 cm^{-1} are observed. The peak at 1712 cm^{-1} belongs to the ester carbonyl group and is shifted to higher energy due to intermolecular hydrogen bonding whereas the peak at 1683 cm^{-1} splits into doublets, retaining the original 1680 cm^{-1} and also creating a new peak at 1650 cm^{-1}. No definite reason for the splitting of the peptide (amide) >C=O group is known; however, a probable explanation is that some of the >C=O groups experience more potential ionic character due to intermolecular aggregation.

In Fig. 8 the FT-IR spectrum of 1% (w/v) solution is shown for different intervals of time after making the solution homogeneous at 100 °C. It is apparent from the figure that the intensity of the 3440 cm^{-1} peak gradually decreases with increase in time at 27 °C and the intensity of the peaks at 3325 and 3309 cm^{-1} gradually increases. One important observation is that initially there was a peak at 3371 cm^{-1} in the solution, however it disappears when the peaks at 3325 and 3309 cm^{-1} begin to develop. This indicates that with time intermolecular aggregation is occurring gradually at this concentration and hence, intensity of the free N–H peaks slowly reduces.

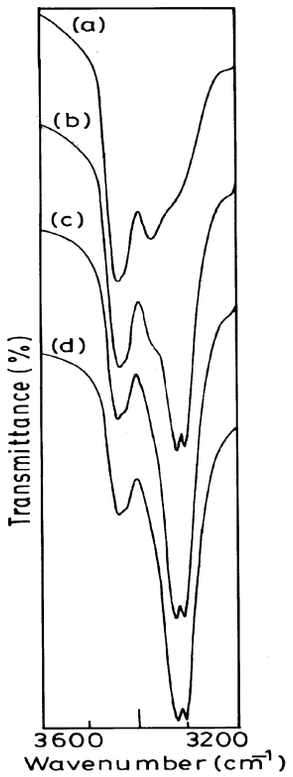

Fig. 8 FT-IR spectra of 1% (w/v) solution in DCB at different time intervals: (a) just after preparation, (b) after 15 minutes, (c) after 1 hour and (d) after 2 hours.

F. Gelation mechanism

Kinetic study of the gelation process is an important tool for understanding the gelation mechanism and both the macroscopic and microscopic mechanism of the gelation process can be elucidated[7,21] from this study. The gelation rate (t_{gel}^{-1}) is usually expressed as a combination of two functions: (I) the concentration function [$f(C)$] and (II) the temperature function [$f(T)$].[7,20c,21]

$$t_{gel}^{-1} \propto f(C)f(T) \quad (5)$$

The macroscopic mechanism of the gelation process can be obtained from the analysis of $f(C)$ whereas the analysis of $f(T)$ yields the microscopic (molecular) mechanism of the gelation process.[7,21] A plot of the gelation rate (t_{gel}^{-1}) with the tripeptide concentration is shown in Fig. 9 for different gelation temperatures (T'_{gel}). At a particular T'_{gel}, the t_{gel}^{-1} increases in a non-linear way for the lower peptide concentration but gradually it levels up at higher concentration. The extrapolation of each

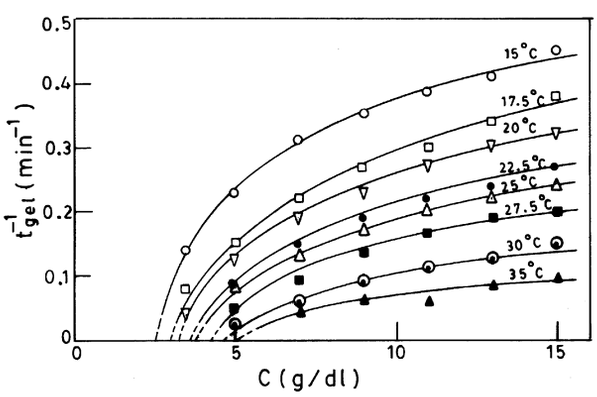

Fig. 9 Plot of gelation rate (t_{gel}^{-1}) with tripeptide concentration in the gel at indicated temperatures.

curve to zero gelation rate yields the critical gelation concentration ($C^*_{t=\infty}$) which is the minimum concentration of tripeptide required to produce the gel at that gelation temperature.

The concentration function: macroscopic mechanism. At a particular gelation temperature

$$t_{gel}^{-1} \propto f(C) \propto \Phi^n \quad (6)$$

where Φ is the reduced overlapping concentration and is expressed as,

$$\Phi = \frac{C - C^*_{t=\infty}(T)}{C^*_{t=\infty}(T)} \quad (7)$$

The 'n' is an exponent and its value can give us an idea about the macroscopic mechanism of the gelation process. According to the percolation theory the gel fraction (G, ratio of gel macromolecules/total number of gel and sol molecules) is expressed as [32,33]

$$G \propto (p - p_c)^\beta \quad (8)$$

where p is the conversion factor during the gelation process and p_c is its critical value, β is a critical exponent and has a value of 0.45 for a three-dimensional lattice. According to the theories of chemical kinetics the reaction rate is proportional to the fraction of molecules overcoming the activation energy barrier. Considering this theory is applicable to the gelation process the gelation rate is directly proportional to the gel fraction.[7,21] An attempt is usually made to measure gelation time as the onset of gelation, but at the gelation threshold the gel fraction (percolation probability) rises very sharply with p.[32,33] So within the error limit of gelation time measurement the gel fraction has some very small but finite value. Consequently:

$$t_{gel}^{-1} \propto G \propto (p - p_c)^\beta \quad (9)$$

Comparing (6) and (9), 'n' may be equal to β (since $C < C^*$ no gelation occurs and $p < p_c$ no percolation occurs).

'n' values are determined from the least squares slope of double-logarithmic plots of t_{gel}^{-1} and Φ (Fig. 10) and are presented in Table 2. From the table it is apparent that the 'n' values vary from 0.44 to 0.54 and they are close to the theoretical value of β, 0.45. So it may be argued that the tripeptide gel in DCB obeys the percolation mechanism in a three-dimensional lattice.

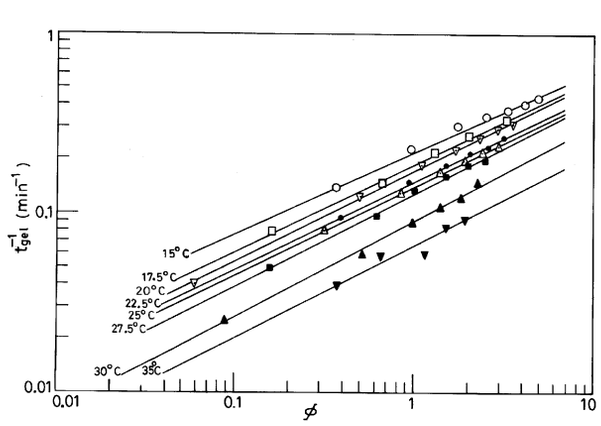

Fig. 10 t_{gel}^{-1} *vs.* Φ (in double logarithmic scale) of tripeptide-gels at indicated temperature.

Microscopic mechanism. The microscopic mechanism of gelation of a tripeptide may be elucidated from the analysis of the temperature coefficient of the gelation rate.[7,21] A tripeptide solution when cooled may form an ordered arrangement (foldamer) by changing the conformation of the bonds and these foldamers then aggregate to produce the crystallites. Also, as evidenced from the phase study as well as from morphological study, liquid–liquid phase separation may also be responsible for the gelation. So the scheme may be represented as:

Table 2 Exponent 'n' values from least squares slopes of log t_{gel}^{-1} *vs.* log Φ plot of tripeptide–DCB gel

Temperature/°C	C^*/g dl^{-1}	'n'
15	2.5	0.44
17.5	3	0.49
20	3.3	0.52
22.5	3.6	0.49
25	3.8	0.50
27.5	4.3	0.52
30	4.6	0.54
35	5.1	0.51
Av	—	0.50
SD	—	0.03

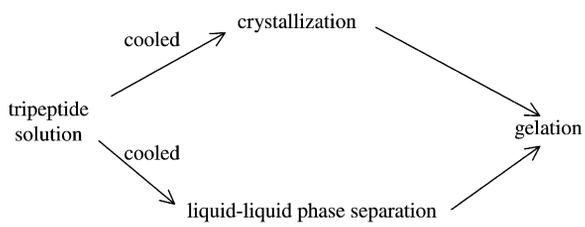

Scheme 1

Crystallites can produce the gel because of rod like morphology, which can easily form network junctions entrapping the solvent. However, the liquid–liquid phase separation is also capable of producing gel as evidenced from the SEM and TEM pictures.[25,26] Scheme 1 indicates the gel formation process of the tripeptide is analogous to the concurrent reaction in chemical kinetics,[34] where the overall rate of disappearance of reactant is a composite of different reaction paths. Assuming this concept of chemical kinetics is applicable to the physical process we have:

t_{gel}^{-1} = crystallization rate + liquid − liquid phase separation rate

In the following section an attempt is made to show how the temperature coefficient analysis of the gelation rate supports Scheme 1.

Crystallization. The growth rate (G) of fibrillar crystals can be expressed as: [35]

$$G = G^0 \exp\left[-\frac{G_a}{kT}\right] \exp\left[-\frac{4l\sigma^2 T_M^0}{kT\Delta H_u^0 \Delta T}\right] \quad (10)$$

Where G^0 is a pre-exponential constant, G_a is the free energy of transport, l is the length of rod, T_M^0 is the equilibrium melting temperature, σ is the surface energy, ΔH_u^0 is the enthalpy of fusion for a perfect crystal, $\Delta T = T_M^0 - T$. Since according to Scheme 1 both the crystallization and liquid–liquid phase separation processes are involved in the gelation process we can equate gelation rate (t_{gel}^{-1}) with the growth rate 'G' of eqn. (10). Then taking the logarithm and rearranging both the equations we have,

$$\ln t_{gel}^{-1} = \text{Const} - \frac{4l\sigma^2 T_{gm}^0}{kT\Delta H_u^0 \Delta T_{gm}} \quad (10a)$$

Now to analyze eqn. (10a) we have to measure ΔT_{gm} and T^{0}_{gm} where T^{0}_{gm} is the equilibrium gel melting temperature. The T^{0}_{gm} may be measured by the Hoffman–Weeks extrapolation procedure[36] and it is shown for 10% (w/v) gel (Fig. 11). In Fig. 12 a

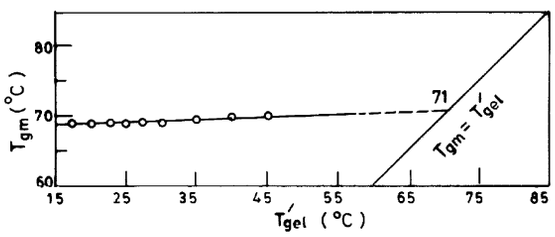

Fig. 11 Hoffman–Weeks plot for the 10% (w/v) tripeptide–DCB gel. [T'_{gel} is the isothermal gelation temperature.]

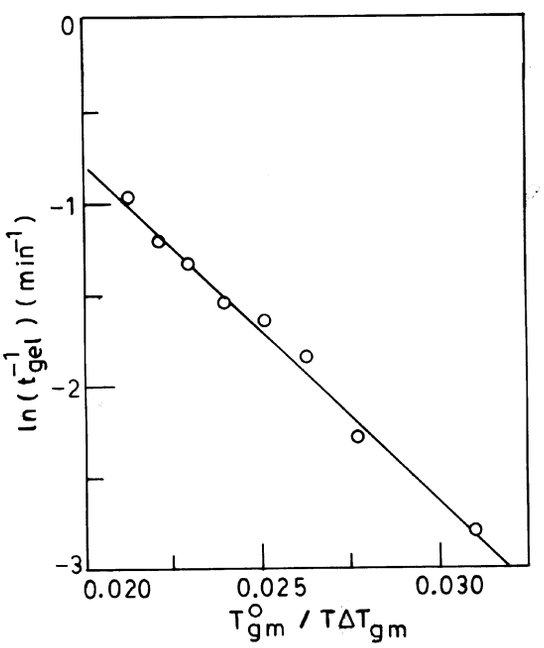

Fig. 12 Ln t^{-1}_{gel} *vs.* $T^{0}_{gm}/T\Delta T_{gm}$ plot for the 10% (w/v) tripeptide–DCB gel.

plot of ln t^{-1}_{gel} has been made with $T^{0}_{gm}/T\Delta T_{gm}$. The straight-line nature of the plot supports crystallization being involved in the gelation process.

Liquid–liquid phase separation. From the SEM and TEM pictures it is apparent that liquid–liquid phase separation is also responsible for the gelation in this system. The liquid–liquid phase separation may occur through spinodal decomposition due to local concentration fluctuation at the gelation temperature and this mechanism is widely accepted for the thermoreversible gelation in certain polymeric systems.[25,26,37] Cahn derived an expression for the most probable wave number of the concentration fluctuation (β_m),[38]

$$\beta_m = \frac{1}{\sqrt{2}}\left[-\frac{1}{2k}\left\{\frac{\delta^2(\Delta F_m/V)}{\delta\phi_1^2}\right\}_{\phi_1^0}\right]^{1/2} \qquad (11)$$

Where k is related to the solute–solvent interaction parameter, $(\Delta F_m/V)$ is the free energy of mixing of a homogeneous solution per unit volume, ϕ_1 is the local concentration and ϕ_1^0 is the average concentration of the solvent. Van Aartsen[39] deduced the temperature dependency of β_m as:

$$\beta_m = L^{-1}\left[3\left(1-\frac{T}{T_s}\right)\right]^{1/2} \qquad (11a)$$

where L is the interaction length, T_s is the spinodal temperature. Under the approximation that liquid–liquid phase separation originates from spinodal decomposition and the frequency of the most probable concentration fluctuation is directly proportional to the gelation rate, eqn. (11a) may be expressed as

$$t^{-1}_{gel} = \frac{c}{L}\left[3\left(1-\frac{T}{T_s}\right)\right]^{1/2} \qquad (12)$$

where 'c' is the proportionality constant. Transforming into the logarithmic form we have:

$$\log t^{-1}_{gel} = \log c' + \frac{1}{2}\log\frac{\Delta T}{T_s} \qquad (12a)$$

Thus a plot of log t^{-1}_{gel} *vs.* log $(\Delta T/T_s)$ should be a straight line with a slope value of 0.5. In Fig. 13 plots of log t^{-1}_{gel} *vs.* log

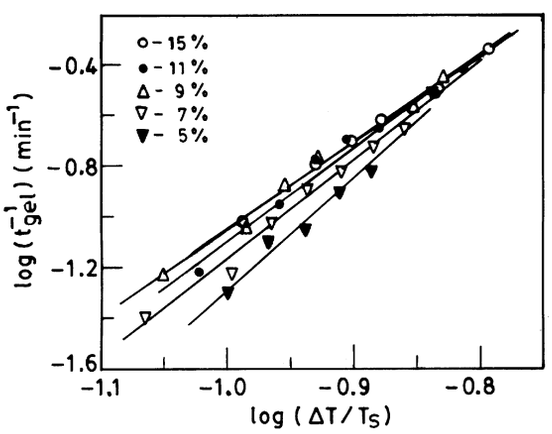

Fig. 13 Log t^{-1}_{gel} *vs.* log $(\Delta T/T_s)$ plot for tripeptide–DCB gels for different tripeptide concentrations.

$(\Delta T/T_s)$ are shown. In this plot T_s is taken from the phase diagram (Fig. 5) determined visually with the approximation that the turbidity disappearance temperature and spinodal temperature are the same. It is clear from the figure that straight lines are obtained as expected from the theory, primarily supporting that spinodal decomposition is also a process of gelation in this system. The least squares slopes of the plots (Fig. 13) are 4.4, 3.9, 3.4, 3.7 and 3.3 for 5%, 7%, 9%, 11% and 15% (w/v) tripeptide gels respectively. So, the slope values are ~7–8 times larger than the theoretical value of 0.5 and the higher slope values may be attributed to the crystallization contribution, indicating that the crystallization mechanism is predominant over the spinodal decomposition for gelation in this system. This proposition appears to be true as evident from the micrographs of Fig. 1 where larger proportions of the fibrillar (crystallite) network than the phase separated network are clearly shown.

Molecular modeling. In this section we want to predict a tentative structure of the tripeptide in the gel. The structure has been developed from a molecular modeling with the MMX program[40] and this is shown in Fig. 14. The structure A has been derived by energy minimizing a molecular structure drawn with the idea that folding may occur at the Aib junction due to the restriction of bond rotation by the presence of bulkier geminal dimethyl groups. The energy minimization results in negative MMX energy and enthalpy values with an intramolecular hydrogen bond between >C=O and H–N< groups near the fold position. The presence of intramolecular hydrogen bonding in the gel state or in the solid state is also evidenced from the FT-IR study discussed earlier. This H-bonding may provide

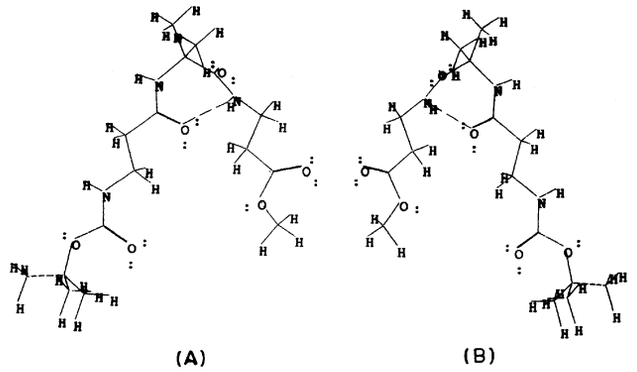

Fig. 14 Molecular modeling of a probable structure of the tripeptide gel in DCB (using MMX program).

additional strength to stabilize the foldamer. The structure B is the mirror image of structure of A. During gelation intermolecular aggregation through hydrogen bonding occurs, as evidenced from the FT-IR study. We therefore propose that structures B and A rest on each other in alternating fashion and hydrogen bonding may occur through the >C=O and >N–H groups. This type of intermolecular aggregation may produce fibrillar or rod like crystal morphology. However, we are unable to give any definite support of this structure from X-ray diffraction data since we have failed to produce any single crystal of this tripeptide.

Conclusion

It appears from the results that the above tripeptide gel in DCB is a unique system where gelation is simultaneously caused by liquid–liquid phase separation and crystallization. The morphology study indicates the simultaneous presence of rod-like and liquid–liquid phase separated networks in the gels. The WAXS study confirms the presence of tripeptide crystallites in the gel state. The thermal study indicates a reversible first-order phase transition and it also predicts the formation of tripeptide–DCB complexation during the gelation. The phase diagrams are also characteristic of liquid–liquid phase separation and tripeptide–solvent complex formation with singular point. The FT-IR study indicates that the gelation occurs due to intermolecular hydrogen bonding. Analysis of the concentration function of the gelation rate of the tripeptide shows that three-dimensional percolation is a suitable model for this system also. The analysis of the temperature function of the gelation rate supports the proposal that (1) crystallization and (2) spinodal decomposition are the probable molecular mechanisms responsible for the gelation.

Experimental

(A) Synthesis of Boc-β-Ala-Aib-β-Ala-OMe

The peptide was synthesized by conventional solution phase methods by using a fragment condensation strategy. The Boc group was used for N-terminal protection and the C-terminus was protected as a methyl ester. Deprotection was performed using saponification. Couplings were mediated by dicyclohexylcarbodiimide–1-hydroxybenzotriazole (DCC–HOBT). All the intermediates were characterized by ^{1}H-NMR (300 and 500 MHz) and thin layer chromatography (TLC) on silica gel and were used without further purification. The final product was purified by column chromatography using silica (100–200 mesh size) gel as stationary phase and ethyl acetate–toluene mixture as eluent. The compound was then fully characterized by 500 MHz ^{1}H-NMR.

(1) Synthesis of Boc-β-Ala-OH. A solution of β-Ala (3.56 g, 40 mmol) in a mixture of dioxan (80 ml), water (40 ml) and 1 M NaOH (40 ml) was stirred and cooled in an ice–water bath. Di-*tert*-butyl pyrocarbonate (9.6 g, 44 mmol) was then added and the stirring was continued at room temperature for 6 h. Then the solution was concentrated *in vacuo* to about 40 to 60 ml, cooled in an ice–water bath, covered with a layer of ethyl acetate (about 50 ml) and acidified with a dilute solution of $KHSO_4$ to pH 2–3 (Congo red). The aqueous phase was extracted with ethyl acetate and this operation was done repeatedly. The ethyl acetate extracts were pooled, washed with water, dried over anhydrous Na_2SO_4 and evaporated *in vacuo*. A white crystalline material was obtained.

Yield: 6.718 g (35.54 mmol, 88.85%). Anal. Calcd. for $C_8H_{15}NO_4$ (189): C, 50.79; N, 7.40; H, 7.9. Found: C, 50.9; N, 7.35; H, 8.12%.

(2) Boc-β-Ala^1-Aib^2-OMe. 5.67 g (30 mmol) of Boc-β-Ala-OH were dissolved in 30 ml dichloromethane (DCM) in an ice–water bath. H-Aib-OMe was isolated from 9.21 g (60 mmol) of the corresponding methyl ester hydrochloride by neutralization using 1 M sodium carbonate solution, with subsequent extraction with ethyl acetate. It was concentrated and 10 ml of it were added, followed immediately by 6.18 g (30 mmol) of dicyclohexylcarbodiimide (DCC). The reaction mixture was allowed to come to room temperature and stirred for 24 h. DCM was evaporated, the residue was taken in ethyl acetate (60 ml), and dicyclohexylurea (DCU) was filtered off. The organic layer was washed with 2 M HCl (3 × 50 ml), brine and then again with 1 M sodium carbonate (3 × 50 ml) and brine (2 × 50 ml). It was dried over sodium sulfate, and evaporated *in vacuo*.

Yield: 7.2 g (25 mmol, 83.33%). Anal. Calcd. for $C_{13}H_{24}N_2O_5$ (288): C, 54.16; H, 8.33; N, 9.72. Found: C, 54.3; H, 8.4; N, 9.7%.

300 MHz ^{1}H NMR ($CDCl_3$, δ ppm): 6.3[Aib(2)NH,1H,s]; 5.2[β-Ala(1)NH,1H,t]; 3.74[OCH_3,3H,s]; 3.36–3.42[β-Ala(2)-C^{α}Hs,2H,m]; 2.37–2.41[β-Ala(2)C^{β}Hs,2H,m]; 1.53[Aib(2)C^{β}-Hs,6H,s]; 1.43 [Boc-CH_3,9H,s].

(3) Boc-β-Ala^1-Aib^2-OH. To 6.62 g (23 mmol) of Boc-β-Ala^1-Aib^2-OMe, 75 ml MeOH and 30 ml of 2 M NaOH were added and the progress of saponification was monitored by thin layer chromatography (TLC). The reaction mixture was stirred. After 10 h methanol was removed under *vacuo*, the residue was taken in 50 ml of water, and washed with diethyl ether (2 × 50 ml). Then the pH of the aqueous layer was adjusted by 2 using 2 M HCl and it was extracted with ethyl acetate (3 × 50 ml). The extracts were pooled, dried over sodium sulfate, and evaporated *in vacuo* to yield 5.48 g of the pure material.

Yield: 5.48 g (20 mmol, 86.9%). Anal. Calcd. for $C_{12}H_{22}N_2O_5$ (274): C, 52.5; H, 8.02; N, 10.2. Found: C, 52.8; H, 8.12; N, 10.02%.

300 MHz ^{1}H NMR [$(CD_3)_2SO$, δ ppm]: 12.01[–COOH,1H,s]; 7.92[Aib(2)NH,1H,s]; 6.55[β-Ala(1)NH,1H,t]; 2.93–2.99[β-Ala(1)C^{α}Hs,2H,m]; 2.06–2.11[β-Ala(1)C^{β}Hs,2H,m]; 1.25[Boc-CH_3s,9H,s]; 1.19[Aib(2)C^{β}Hs,6H,s].

(4) Boc-β-Ala^1-Aib^2-β-Ala^3-OMe. 4.11 g (15 mmol) of Boc-β-Ala-Aib-OH in 20 ml of DMF was cooled in an ice–water bath. H-β-Ala-OMe was isolated from 4.18 g (40 mmol) of the corresponding hydrochloride by neutralization, with subsequent extraction with ethyl acetate and it was concentrated. 10 ml of the concentrated material were added, followed immediately by 3.09 g (15 mmol) DCC and 2.0 g (15 mmol) of 1-hydroxybenzotriazole (HOBT). The reaction mixture was stirred for three days. The residue was taken in ethyl acetate (60 ml) and the DCU was filtered off. The organic layer was then washed with 2 M HCl (3 × 50 ml), brine, 1 M sodium carbonate (3 × 50 ml) and again with brine (2 × 50 ml), dried over anhydrous sodium sulfate and evaporated *in vacuo* to yield 3.59 g (10 mmol) of white solid. Purification was done by silica gel column (100–200 mesh size) using ethyl acetate as eluant. Yield 68.3%.

Anal. Calcd. for $C_{16}H_{29}N_3O_6$ (359): C, 53.8; H, 8.07; N, 11.69. Found: C, 53.6; H, 8.12; N, 11.52%.

500 MHz ^{1}H NMR ($CDCl_3$, δ ppm): 6.94[β-Ala(3)NH,1H,t]; 6.27[Aib(2)NH,1H,s]; 5.59[β-Ala(1)NH,1H,t]; 3.7[–OCH_3, 3H,s]; 3.49–3.52[β-Ala(3)C^{α}Hs,2H,m]; 3.37–3.40[β-Ala(1)-C^{α}Hs,2H,m]; 2.57–2.59[β-Ala(3)C^{β}Hs,2H,m]; 2.40–2.42-[β-Ala(1)C^{β}Hs,2H,m]; 1.51[Aib(2)C^{β}Hs,6H,s]; 1.44[Boc-CH_3, 9H,s].

(B) NMR studies

All NMR experiments were performed on Bruker DRX 500 MHz and DPX 300 MHz spectrometers. A phase sensitive DQF-COSY experiment was done for sequence specific assignments by collecting 2k data points in f2 and 512 points in f1. Quadrature detection in f1 was achieved using TPPI. Data were processed on silicon Graphics using Bruker XWIN NMR software. Typically, a Qsine-Squared Window function was applied in both dimensions, with Zero filling in f2 to 512 points. NMR chemical shifts and line widths were shown to be independent of tripeptide concentration in the range 40 to 0.25 mM, which strongly suggested that the tripeptide didn't aggregate for the above range of concentration.

(C) Mass spectroscopy

The mass spectrum of the tripeptide was taken using the MALDI-MS spectroscopic technique. The spectrum was scanned over the mass range of *m*/*z* 100–1000 by 0.1 amu, with dwell time 1 ms per step.

(D) FT-IR spectroscopy

The FT-IR spectra were taken using a Shimadzu (Japan) model FT-IR spectrophotometer with a sample-shuttle device, averaging over 40 scans. Solvent (DCB) spectra were obtained under the same conditions using a cuvette with 1 mm path length. A Nicolet FT-IR instrument [Magna IR-750 spectrometer (series II)] was used to obtain the solid state and the gel state FT-IR spectra. The solvent spectrum was subtracted from the gel spectra to obtain tripeptide spectra in the gel state.

(E) Preparation of gel

The gels were prepared in two ways. (1) For morphology and structural investigations, the gels were prepared in glass tubes (6 mm id) by taking an appropriate amount of the tripeptide sample and 1,2-dichlorobenzene (DCB) [S.D. Chemicals, India, Analytical Reagent Grade]. The tubes were degassed by the repeated freeze–thaw technique and were then sealed under vacuum (10^{-3} mm Hg.). They were made homogeneous at 110 °C and then quickly gelled by quenching at room temperature (30 °C). (2) For the thermal investigation, the gels were prepared in Perkin-Elmer large volume capsules (LVC) by taking appropriate amounts of tripeptide and the solvent and were tightly sealed with the help of a quick press. They were made homogeneous by keeping them at 110 °C for 10 minutes and were gelled at 15 °C for 3 h by cooling from 110 °C at the rate of 200 °C min^{-1}.

(F) Morphology and structural investigations of the gels

The morphology of the gels was investigated using optical microscopy (OM), transmission electron microscopy (TEM) and scanning electron microscopy (SEM). The optical microscopy of the samples was done using a small amount of the gel on microscopic slides and drying in a stream of air at room temperature. The sample was observed under the microscope. The morphology of the undried gel was also observed in the microscope using polarized light which facilitated observation of the crystallites. For SEM study the 10% (w/v, *i.e.*, 10 g of tripeptide in 100 ml of solvent) gels were dried in vacuum for three days at room temperature and were gold coated. SEM pictures were then taken in an SEM apparatus (Hitachi S-415A). The TEM study was done by dropping a 0.3% (w/v) solution of the tripeptide in 1,2-dichlorobenzene directly on a carbon coated copper grid which was dried in vacuum at 30 °C for three days. The grid was then observed in a transmission electron microscope (Hitachi H-600), both in the transmission mode and in the diffraction mode. The structural investigation of the gels was done by wide angle X-ray scattering (WAXS) and Fourier transform infra-red spectroscopy. In the WAXS study the gels were dried in vacuum at 30 °C for 5 days and the diffractograms were recorded in a Phillips powder diffraction apparatus (model PW1710). Nickel-filtered Cu-Kα radiation was used for this purpose. The gel was taken in a glass groove and the diffractogram was recorded at the step scan with the step size of 0.02°, 2θ and a time per step of 0.8 s. The type of scan was continuous.

(G) Thermal study

The thermal studies of the gels were done in a differential scanning calorimeter (DSC-7, Perkin-Elmer). The tripeptide and DCB in the required amounts were taken in Large Volume Capsules (LVCs) fitted with an O-ring and these were tightly sealed with the help of a quick press. They were kept at 110 °C for 10 minutes to make them homogeneous and cooled at 15 °C and equilibrated for 3 h to produce the gels. The LVC pans were then heated at the rate of 10 °C min^{-1} and thermograms were recorded. For cooling, after equilibration at 110 °C for 10 minutes, the samples were cooled at the rate of 5 °C min^{-1} and thermograms were recorded. For the isothermal gelation at different temperatures the samples were cooled from 110 °C to the desired isothermal temperatures and kept there for 3 h. They were heated at the scanning rate of 10 °C min^{-1} from that temperature without cooling. The melting point, gelation temperature and the corresponding enthalpy changes were measured using a computer attached to the instrument. The DSC was calibrated with indium before each set of experiments.

(H) Gelation rate measurement

The kinetics of the gelation were studied by measuring the gelation time using the test tube tilting method.[7,20–21] To make gels at different tripeptide concentrations 0.2 ml of 1,2-dichlorobenzene (density = 1.304 g ml^{-1}) and an appropriate amount of the tripeptide (7–30 mg) were taken in glass tubes (6 mm id and 1 mm thickness). They were degassed by a repeated freeze–thaw technique and were sealed under vacuum (10^{-3} mm Hg). They were homogenized at 100 °C and were quickly transferred to a thermostatic bath set at a predetermined temperature. The gelation time (t_{gel}) was counted as the time where no flow occurred after the tube was tilted.[7,20–21] Accuracy in the rate measurement to t_{gel} = ±5 s was achieved by a trial and error procedure.[7,21] The inverse of the gelation time was approximated as the gelation rate (t_{gel}^{-1}).[7,20,21]

Acknowledgements

One of the authors (A. B.) acknowledges the Department of Science and Technology, New Delhi, for financial support.

References

1 (*a*) J. H. van Esch and B. L. Feringa, *Angew. Chem., Int. Ed.*, 2000, **39**, 2263; (*b*) F. S. Schoonbeek, J. H. van Esch, R. Hulst, R. M. Kellogg and B. L. Feringa, *Chem. Eur. J.*, 2000, **6**, 2633; (*c*) J. H. van Esch, F. S. Schoonbeek, M. de Loos, H. Kooijman, A.-L. Spek, R. M. Kellogg and B. L. Feringa, *Chem. Eur. J.*, 1999, **5**, 537.

2 P. Terech and R. G. Weiss, *Chem. Rev.*, 1997, **97**, 3133.
3 T. D. Clark, L. K. Buehler and M. R. Ghadiri, *J. Am. Chem. Soc.*, 1998, **120**, 651.
4 (*a*) D. Philip and J. F. Stoddart, *Angew. Chem., Int. Ed. Engl.*, 1996, **35**, 1154; (*b*) O. Gronawald and S. Shinkai, *J. Chem. Soc., Perkin Trans. 2*, 2001, 1933; (*c*) J. H. Jung, M. Amaike, K. Nakashima and S. Shinkai, *J. Chem. Soc., Perkin Trans. 2*, 2001, 1938.
5 M. S. Vollmer, T. D. Clark, C. Steinem and M. R. Ghadiri, *Angew. Chem., Int. Ed.*, 1999, **38**, 1598.
6 *Comprehensive Supramolecular Chemistry, Vol. 6: Solid-State Supramolecular Chemistry: Crystal Engineering*, Eds. D. D. MacNicol, F. Toda and R. Bishop, Elsevier, Oxford, UK, 1996.
7 S. Mal and A. K. Nandi, *Polymer*, 1998, **30**, 6301.
8 A. K. Dikshit and A. K. Nandi, *Macromolecules*, 1998, **31**, 8886.
9 K. Hanabusa, M. Yamada, M. Kimura and H. Shirai, *Angew. Chem., Int. Ed. Engl.*, 1996, **35**, 1949.
10 R. J. H. Hafkamp, M. C. Feiters and R. J. M. Nolte, *J. Org. Chem.*, 1999, **64**, 412.
11 Y.-C. Lin, B. Kachar and R. G. Weiss, *J. Am. Chem. Soc.*, 1989, **111**, 5542.
12 S. H. Gellman, *Acc. Chem. Res.*, 1998, **31**, 173.
13 (*a*) D. H. Appella, L. A. Chistianson, D. A. Klein, D. R. Powell, Y. Huang and S. H. Gellman, *Nature*, 1997, **387**, 381; (*b*) X. Wang, J. F. Espinosa and S. H. Gellman, *J. Am. Chem. Soc.*, 2000, **122**, 4821.
14 (*a*) S. Abele, D. Guichard and D. Seebach, *Helv. Chim. Acta*, 1998, **81**, 2141; (*b*) D. H. Appella, L. A. Chistianson, I. L. Karle, D. R. Powell and S. H. Gellman, *J. Am. Chem. Soc.*, 1999, **121**, 6206.
15 (*a*) Y. J. Chung, B. R. Huck, L. A. Christianson, H. E. Stanger, S. Krauthauser, D. R. Powell and S. H. Gellman, *J. Am. Chem. Soc.*, 2000, **122**, 3995; (*b*) D. Seebach, S. Abele, K. Gademan and B. Jaun, *Angew. Chem., Int. Ed.*, 1999, **38**, 1595.
16 (*a*) M. R. Ghadiri, J. R. Granja, R. A. Milligan, D. E. McRee and N. Jhazanovich, *Nature*, 1993, **366**, 324; (*b*) M. R. Ghadiri, J. R. Granja and L. K. Buchler, *Nature*, 1994, **369**, 301; (*c*) H. S. Kim, J. D. Hartgerink and M. R. Ghadiri, *J. Am. Chem. Soc.*, 1998, **120**, 4417.
17 (*a*) D. Raganathan, V. Haridas, S. Kumar, A. Thomas, K. P. Madhusudanam, R. Nagraj, A. C. Kumar, A. V. S. Sarma and I. L. Karle, *J. Am. Chem. Soc.*, 1998, **120**, 8448; (*b*) D. Ranganathan, V. Haridas, R. Gilardi and I. L. Karle, *J. Am. Chem. Soc.*, 1998, **120**, 10793.
18 (*a*) S. Mal and A. K. Nandi, *Langmuir*, 1998, **14**, 2238; (*b*) A. K. Dikshit and A. K. Nandi, *Macromolecules*, 2000, **33**, 2616.
19 (*a*) I. L. Karle, A. Banerjee, S. Bhattacharyya and P. Balaram, *Biopolymers*, 1996, **38**, 515; (*b*) A. Banerjee, S. Datta, A. Pramanik, N. Shamala and P. Balaram, *J. Am. Chem. Soc.*, 1996, **118**, 9477.
20 (*a*) H. M. Tan, A. Hiltner, A. Moet and E. Baer, *Macromolecules*, 1983, **16**, 28; (*b*) A. Prasad and L. Mandelkern, *Macromolecules*, 1990, **23**, 5041; (*c*) M. Ohkura, T. Kaniaya and K. Kaji, *Polymer*, 1992, **33**, 5044; (*d*) J. W. Cho, H. Y. Song and S. Y. Kim, *Polymer*, 1993, **34**, 1024.
21 (*a*) S. Mal, P. Maiti and A. K. Nandi, *Macromolecules*, 1995, **28**, 2371; (*b*) S. Malik, T. Jana and A. K. Nandi, *Macromolecules*, 2001, **34**, 275.
22 In the electronic diffraction pattern some spots are also seen; the formation of single crystals in the gelation condition is a difficult situation and a probable reason for the simultaneous occurrence of rings and spots is the different sizes of the crystals. The upper size limit giving ring patterns is 10^3–10^2 Å but above this size electron diffraction may give spots[23,24].
23 K. W. Andrews, D. J. Dyson and S. R. Keown, *Interpretation of Electron Diffraction Patterns*, Plenum Press, New York, 1964.
24 T. Jana and A. K. Nandi, *Langmuir*, 2000, **16**, 3141.
25 H. Berghmans, in *Integration of Fundamental Polymer Science and Technology*, Eds. P. J. Lemstra and L. A. Kleintjens, Elsevier Applied Science, London, 1988, Vol. 2, p. 296.
26 R. M. Hiknet, S. Callister and A. Keller, in *Integration of Fundamental Polymer Science and Technology*, Eds. P. J. Lemstra and L. A. Kleintjens, Elsevier Applied Science, London, 1988, Vol. 2, p. 306.
27 C. Daniel, C. Dammer and J. M. Guenet, *Polym. Commun.*, 1994, **35**, 4243.
28 J. M. Guenet and G. B. Mckenna, *Macromolecules*, 1998, **21**, 1752.
29 A. Reisman, *Phase Equilibria*, Academic Press, New York, 1970.
30 J. R. Dyer, *Application of Absorption Spectroscopy of Organic Compounds*, Prentice Hall of India, New Delhi, 1987.
31 N. B. Colthup, L. H. Daly and S. E. Wilberley, *Introduction to Infrared and Raman Spectroscopy*, Academic Press, New York, 1964.
32 D. Stauffer, A. Coniglio and M. Adam, in *Advances in Polymer Science*, Ed. K. Dusek, Springer-Verlag: Berlin, 1982, Vol. 44, p. 103.
33 R. Zallen, *The Physics of Amorphous Solids*, John Wiley & Sons, New York, 1983, p. 135.
34 S. W. Benson, *The Foundation of Chemical Kinetics*, McGraw-Hill Book Co., New York, 1960, p. 26.
35 A. J. Pennings, *J. Polym. Sci., Polym. Symp.*, 1977, **59**, 55.
36 J. D. Hoffman and J. J. Weeks, *J. Res. Natl. Bur. Stand. (U. S.)*, 1962, **66**, 13.
37 (*a*) D. Asnaghi, M. Cigilo, A. Bossi and P. G. Righetti, *J. Chem. Phys.*, 1995, **102**, 9376; (*b*) R. Bansil, J. Lal and B. L. Carvalho, *Polymer*, 1992, **33**, 2961; (*c*) H. Takeshita, T. Kanaya, K. Nishida and K. Kaji, *Macromolecules*, 1999, **32**, 7815.
38 J. W. Cahn, *J. Chem. Phys.*, 1965, **42**, 93.
39 J. J. Van Aartsen, *Eur. Polym. J.*, 1970, **6**, 919.
40 K. E. GaJewski and M. H. Gillberr, in *Advances in Molecular Modeling*, Ed. D. Liotta, JAI Press, Greenerick, CT, 1990, Vol. 2.